

# Numerical MHD Simulation of the Coupled Evolution of Collisional Plasma and Magnetic Field in the Solar Chromosphere. I. Gradual and Impulsive Energisation

*Solar Physics*

L.M. Alekseeva<sup>1</sup> · S.P. Kshevetskii<sup>2</sup>

© Springer ●●●

**Abstract** The dynamical coupling between the solar chromospheric plasma and magnetic field is investigated by numerically solving a fully self-consistent, two-dimensional initial-value problem for the nonlinear collisional MHD equations including electric resistivity, thermal conduction, and, in some cases, gas-dynamic viscosity. The processes in the contact zone between two horizontal magnetic fields of opposite polarities are considered. The plasma is assumed to be initially motionless and having a temperature of 50,000 K uniform throughout the plasma volume; the characteristic magnetic field corresponds to a plasma  $\beta \gtrsim 1$ . In a physical-time interval of 17 seconds typically covered by a computational run, the plasma temperature gradually increases by a factor of two to three. Against this background, an impulsive (in 0.1 seconds or less) increase in the current-aligned plasma velocity occurs at the site of the current-layer thinning (sausage-type deformation, or  $m = 0$  pinch instability). Such a “velocity burst” can be interpreted physically as an event of suprathermal-proton generation. Further development of the sausage instability results in an increase in the kinetic temperature of the protons to high values, even to those observed in flares. The form of our system of MHD equations indicates that such increases are a property of the exact solution of the system at an appropriate choice of the parameters. Magnetic reconnection does not manifest itself in this solution: it would generate flows forbidden by the chosen geometry. Therefore, the pinch-sausage effect can act as an energiser of the upper chromosphere and be an alternative to the magnetic-reconnection process as the producer of flares.

---

✉ L.M. Alekseeva  
l.m.alekseeva@yandex.ru  
S.P. Kshevetskii  
renger@mail.ru

<sup>1</sup> Skobeltsyn Institute of Nuclear Physics, Lomonosov Moscow State University, Moscow, 119991 Russia

<sup>2</sup> Immanuel Kant Baltic Federal University, Kaliningrad, 236041 Russia

---

**Keywords:** Magnetohydrodynamics; Plasma Physics; Magnetic fields; Chromosphere; Heating, Chromospheric; Transition Region; Jets; Energetic Particles, Protons

## 1. Introduction

The chromosphere is much less studied than the underlying photosphere and overlying corona. However, its properties are widely discussed in the context of the fundamental problems of solar physics (Aschwanden, 2004; Fletcher *et al.*, 2010). Much effort has been made to understand the mechanism of heating of the upper chromosphere and corona. Such a mechanism is usually associated with coronal processes at plasma-parameter values  $\beta < 1$ . On the other hand, some observed phenomena lead, as Aschwanden notes, “to a paradigm shift from the coronal heating problem to a dynamic chromospheric energisation problem” (Aschwanden, 2001); the latter corresponds to the case of  $\beta \geq 1$  (Aschwanden and Nightingale, 2005; Aschwanden, 2008). Therefore, particular attention should be given to plasma properties at  $\beta \approx 1$ .

Progress in understanding these issues will remain slow as long as the knowledge of the chromosphere remains fragmentary. In many cases, detailed information provided by the modern high-resolution instruments can hardly be compared with theoretical conclusions, since the theories are based on non-observable parameters (nonpotential magnetic field, magnetic stress or twist, electric fields, *etc.*) (Aschwanden, 2008).

Such difficulties in studying the dynamics of the chromospheric plasma itself could be avoided using the completely self-consistent system of MHD equations. Various quantities are mutually related in a solution of this system, and a passage from some quantity crucial for the process to another, more convenient for an observer, can be done quite routinely.

However, in the practice of simulations of the chromospheric plasma, even the inclusion of magnetic fields increases enormously the level of complexity (Carlson, 2007). Highly dynamic, nonlinear processes are typical of the chromosphere. Small scales are involved in them due to both turbulent chaos and the formation of shock fronts. Aschwanden (2004) writes that “typical difficulties with the MHD method are the same as they are typical for numerical simulations, such as heavy computing demand, convergence problems, insufficient spatial resolution to handle discontinuities, line-tying (continuous slippage of magnetic-field lines)”.

However, direct simulations of dynamical coupling between laboratory ion–electron plasma and magnetic field were made by numerically solving a two-dimensional initial-value problem for fully self-consistent, nonlinear collisional MHD equations, which give a unified description for  $\beta > 1$ ,  $\beta \approx 1$ , and  $\beta < 1$  (Brushlinskii and Morozov, 1980; Brushlinsky, 1989). Later, various situations were considered in the context of studying laboratory plasma-channel flows (see an overview by (Alekseeva, 2006)). It is worthwhile to try to comprehend how the features of the dynamical coevolution of the plasma and magnetic field, revealed in this way, can manifest themselves under solar conditions. To this

end, we solve here numerically an initial-value problem of this sort; in so doing, as in Brushlinskii and Morozov (1980), we do not assume any properties of the solutions sought for. In view of investigating the solar-plasma dynamics, we employ a substantially improved numerical technique. This makes it possible to describe small-scale turbulence and discontinuities, automatically passing, whenever necessary, to the use of the class of generalised functions. This technique was verified in our previous studies (Kshevetskii and Gavrilov, 2005; Kshevetskii, 2006; Alekseeva and Kshevetskii, 2006, 2011)). This allows us to obtain solutions for comparatively long time intervals even if small-scale perturbations develop.

We consider a two-dimensional problem assuming that all physical quantities are constant along the magnetic-field lines and the magnetic field is horizontal. This is motivated by the fact that about 95% of the magnetic flux issuing from the photosphere closes below the coronal heights (Priest, 1982; Aschwanden, 2004), so that the magnetic field in the chromosphere consists largely of horizontal apical segments of the field lines; horizontal segments are also present in the field lines of the magnetic canopies.

We investigate here the coevolution of the collisional electron–proton plasma and magnetic field at the characteristic plasma parameter values  $\beta_{0*} = 1.5$ , 1.6, or 2.3, which are present in the upper chromosphere (Gary, 2001) [see also Figure 1.22 in Aschwanden (2004)]. Our MHD simulations are carried out under the assumption that the plasma is initially motionless and has a temperature of 50,000 K everywhere in the computation domain.

Such fully ionized plasma can be attributed to the upper chromosphere. The upper boundary of the chromospheric layer is typically associated with a temperature of about 50,000 K; this layer is assumed to be overlaid with a transition region, which, in turn, changes into the corona at temperatures of about 500,000 K (Gabriel, 1994). However, more recent observations modified our understanding of the geometry of the solar atmosphere, which is now regarded as an inhomogeneous mixing of photospheric, chromospheric, and coronal zones produced by various dynamic processes (Schrijver, 2001) [see also Figure 1.17 of Aschwanden (2004)]. Since we consider small-size regions, there is generally no need to attribute them to particular layers, and the temperature can be assumed to be the basic parameter characterising the plasma under study.<sup>1</sup>

Alekseeva and Kshevetskii (2011) carried out simulations for a characteristic plasma-  $\beta_{0*} = 1.5$  and an initial magnetic configuration consisting of two regions with oppositely directed magnetic fields. We noted the development of a pinch-type plasma instability. Some its features are also observed in laboratory plasmas; these are the contraction of the current layer as a whole, the local thinning (sausage-type deformation) of the stagnated current layer, and the development of oppositely directed, current-aligned plasma streams. However, the process in an unbounded solar plasma proved to be more complex. Another pair of jets accompanied by a strip of small-scale inhomogeneities was

---

<sup>1</sup>To avoid misunderstanding, it is worth noting that the definition of the upper chromosphere used by Gabriel (1994) is not the one in common usage, and there are also other different definitions, usually based on the characteristics of neutral-particle distributions over the solar atmosphere. We can generally consider plasma with temperatures of above 20,000 K using the equations for the fully ionised gas.

directed transversely to the electrical current. As viewed along the magnetic-field lines, the pattern of field, velocity, and density distributions appeared to be cross-shaped; we shall call such a pattern a *transient “cross-shaped” structure*. The jet velocity exceeded  $20 \text{ km s}^{-1}$ . A class of situations was identified in which the plasma temperature increased in the central part of this pattern (the computations were terminated when it doubled).

Here, we shall demonstrate that impulsive processes can develop against the background of a gradual development of this pattern (which will be illustrated in the case of  $\beta_{0*} = 1.6$ ). Specifically, intense plasma streams emerge in a temporal interval of about 0.1 second. Such a *velocity burst* can physically be interpreted as an event of suprathermal-ion generation. The kinetic temperature based on the maximum velocity can reach about 0.5 MK. This is indicative for the dynamic energisation of a parcel of chromospheric plasma to coronal temperature. We conclude that the velocity burst is due to a sausage-type pinch instability. This velocity peak is neither unique nor the highest one. The very form of the initial-value problem considered here indicates an important property of its exact solution: the development of the sausage instability ultimately results in an infinite growth of the plasma velocity  $[v]$  with time  $[t]$ , which implies an increase in the kinetic temperature to high values, even such as observed in flares. Our numerical solutions allow us to trace this process.

The infinite velocity growth can naturally be suppressed by gas-dynamic molecular viscosity, which will be observed in simulations with a strongly exaggerated viscosity. Some other factors may also act similarly. Analyses of their role fall beyond the scope of our study. We are interested in investigating the possibility of impulsive plasma energisation by the pinch instability and, following Carlsson (2007), “perform numerical experiments and modelling in simplified cases in order to fashion a basic physical foundation upon which to build our understanding.”

## 2. Magnetohydrodynamic Background

### 2.1. Collisional Plasma and its Dynamical Properties Depending on the Rarefaction Degree

Some particular phenomena known in the theory of accelerating plasma channels may be of interest to solar physics. Two-dimensional flows transverse to the magnetic field with the physical quantities constant along the magnetic-field lines have long been studied. Early numerical simulations – generally, with a finite electric conductivity and the Hall effect taken into account – discovered the development of closed solitary electric-current structures, i.e. isolated magnetic tubes (Alekseeva and Solov’ev, 1964; Brushlinskii, Gerlakh, and Morozov, 1968; Morozov and Solov’ev, 1980; Brushlinskii and Morozov, 1980). Without the Hall effect, they develop at  $\beta \geq 1$ , and they do not depend on the presence of walls confining the plasma (Alekseeva and Solov’ev, 1964; Morozov and Solov’ev, 1980; Brushlinskii and Morozov, 1980). The role of the Hall effect in the dynamics of a

dense plasma with a magnetic field is determined by the dimensionless parameter

$$\xi = c(eL)^{-1} \sqrt{m_i / (4\pi N_*)}, \quad (1)$$

which will be referred to as the Hall-plasma-dynamics parameter; here,  $c$ ,  $m_i$ ,  $L$ , and  $N_*$  are, respectively, the speed of light, the proton mass, the length scale, and the reference concentration of particles of the a given electrical-charge sign. The plasma is assumed to be quasi-neutral, with a large but finite  $N_*$  (Brushlinskii and Morozov, 1980). In a Hall plasma, although structures of the above-mentioned sort arise at  $\beta > 1$ , they manifest themselves more clearly (and with sharper gradients), as  $\beta$  decreases, being related to explosive events characteristic of Hall plasmas (Brushlinskii and Morozov, 1980). These phenomena are, to all appearance, due to a global gradient of the gas pressure in the flow direction (Alekseeva and Solov'ev, 1964; Brushlinskii and Morozov, 1980; Alekseeva, 1997a,b, 1999).

In the solar atmosphere, the Boltzmann-distribution-based pressure gradient can produce similar phenomena. A stationary two-dimensional solution of the same equation system was found analytically for the case of a very weak magnetic field in a Hall plasma with the presence of gravity (Alekseeva, 2006). It represents a thin layer of a current directed upward, with a downward plasma flow and a slower return flow at the periphery of this layer. It changes into a thin current sheet in a more rarefied plasma, which may be of interest in the context of magnetic reconnection. Goodman (2005) used a steady-state MHD model of the collisional chromospheric Hall plasma, with the electrical-conductivity and thermoelectric tensors taken into account in Ohm's law. For special conditions of a given magnetic field of a current-layer type and a given bulk plasma flow orthogonal to the magnetic field, he found that the plasma thermodynamic parameters in a certain part of the current layer correspond to the lower-corona range.

These results prompted us to start a systematic numerical investigation based on the collisional MHD equations for fully ionised chromospheric layers, generally with the inclusion of gravity, the Hall effect, and time-dependent electric and thermal conduction. To solve an axisymmetric or planar-symmetric initial-value problem, we applied a special numerical method (Kshevetskii and Gavrilov, 2005) that uses generalised functions wherever necessary, to the solar plasma.

## 2.2. MHD Chromospheric Processes in our Two-Dimensional Numerical Simulations

The penetration of the magnetic field into the chromosphere immediately and typically entails i) a tendency of the gas pressure and magnetic pressure to come into balance and ii) the interaction between the penetrating magnetic field and other closely located chromospheric magnetic fields. Generally, the two phenomena parallel each other and both produce wavelike steadying processes (from here on, referred to as *primary waves*), which interfere.

We investigate this typical situation for the case of two contacting magnetic regions of opposite polarities. (For simplicity, we choose the initial distributions

of the variables to be symmetric with respect to the zero-field surface. We also assume the physical quantities to be constant along the magnetic-field lines, which are horizontal, straight and parallel; therefore, a 2D problem can be formulated.) In this circumstances, the primary waves associated above with phenomenon ii) are due to electrical-current contraction in the plasma medium and are formed by the compression and subsequent expansion of the whole current zone between the regions. Also, a sausage instability similar to that in the laboratory Z-pinch can be expected at some locations in the same zone, in the presence of the primary steadying waves and/or after they recede.

Our numerical method allows us to calculate inhomogeneities (waves, turbulence, and shocks) spontaneously arising during the nonlinear process of plasma and magnetic-field coevolution. We do this without anticipating any properties of the solution. Thus, solving an initial-value problem for the fully consistent system of MHD equations, we can perform direct numerical simulations specifying only the initial conditions.

Our early simulations at  $\xi \neq 0$  or, in other words, taking into account the Hall effect and gradient of electron pressure showed that the process modeled is highly dynamical and complex (Alekseeva and Kshevetskii, 2006) and it is virtually impossible to distinguish between the contributions of different phenomena to the observed scenarios. The difficulties can be overcome only by a stepwise consideration of progressively more complex situations. Here, as in Alekseeva and Kshevetskii (2011), we omit the Hall effect and electron-pressure terms in the equations [i.e. we use the system of equations referred to as the standard MHD model (see, e.g., Leake and Arber, 2006)].

Thus, at least three groups of physical phenomena can manifest themselves in our direct simulations: primary waves of steadying processes, pinch sausage instability and turbulence of various kinds, including small-scale waves and shocks due to the nonlinearity of the processes.

Simulations by Alekseeva and Kshevetskii (2011) revealed a time interval during which cross-shaped transient structures are present. Here, we use a higher-accuracy algorithm to demonstrate that the transient structures can be accompanied by impulsive generation of suprathermal protons in a manner similar to the formation of proton beams in a laboratory Z-pinch.

To conclude this section, it is worth noting that our approach differs from those typically adopted. Many researchers avoid considering the effects of spontaneously developing small-scale turbulence, waves and shocks because of severe difficulties entailed by such efforts.<sup>2</sup> In contrast, our method is specifically tailored for describing small-scale inhomogeneities irrespective of their scale.

---

<sup>2</sup>For example, Leake and Arber (2006), noting the difficulties with the inclusion of small-scale effects in direct large-scale MHD simulations, artificially introduce a sort of relaxation – in particular, to suppress unresolved acoustic modes, thermal conduction and shock dissipation on small scales. In this way, they succeed in their simulations with chromospheric neutral particles taken into account.

### 3. Mathematical Formulation of the Problem

#### 3.1. The System of MHD Equations

To nondimensionalise the variables, we use two basic units, viz. the number density  $[N_*]$  of either component of the quasi-neutral proton–electron plasma and the plasma temperature  $[T_*]$ , which is characteristic of a certain layer of the solar atmosphere before the arrival of the magnetic field and refers to the nonmagnetic regions after the field arrival. Then  $\rho_* \equiv m_i N_*$  will be the unit density. We also choose the scale height of the atmosphere  $[H = kT_*/(m_i g)]$  (where  $k$  is the Boltzmann constant and  $g$  is the gravitational acceleration) as the unit length  $L$ .

Our problem consists in studying the processes that can occur in such a layer under the influence of a magnetic field. As a unit magnetic field, we use its characteristic magnitude  $[B_0]$ . Then the combinations  $B_0^2/(4\pi)$  and  $v_{0*} \equiv B_0/\sqrt{4\pi\rho_*}$  can be used as the unit pressure and velocity, respectively. We choose  $t_{0*} \equiv H/v_{0*}$  as the unit time and  $cB_0/(4\pi H)$  as the unit of the electric current. Thus, all of the units are specified, given the dimensional quantities  $T_*$ ,  $N_*$ , and  $B_0$ .

However, we should keep in mind that the response of the plasma medium to the initially present magnetic field (with a characteristic value of  $B_0$ ) can conveniently be judged by the value of the plasma- $\beta$  parameter,

$$\beta_{0*} = 8\pi\mathcal{P}_*/B_0^2; \quad (2)$$

it gives a general characterisation of the situation, being the ratio of the characteristic dimensional pressures—the gas pressure  $\mathcal{P}_* = kN_*T_*$  to the magnetic pressure  $B_0^2/8\pi$ . We write  $B_0$  and, accordingly,  $v_{0*}$  in terms of  $\beta_{0*}$  (recall that  $T_*$  and  $N_*$  do not depend on the magnetic field) as

$$B_0 = \beta_{0*}^{-1/2} \sqrt{8\pi k N_* T_*}, \quad (3)$$

$$v_{0*} = \beta_{0*}^{-1/2} \sqrt{2kT_*/m_i}, \quad (4)$$

to express all the introduced units in terms of  $T_*$ ,  $N_*$ , and  $\beta_{0*}$ .

We restrict ourselves to a two-dimensional geometry and assume that the physical quantities do not vary along the straight, parallel, horizontal magnetic-field lines, and the plasma motion is directed across them. In this case, the complete system of self-consistent nonlinear equations of collisional magnetogas-dynamics with allowances for finite electrical resistance, thermal conductivity, and plasma gas-dynamical viscosity (Brushlinskii and Morozov, 1980; Braginskii, 1965), written in terms of the dimensionless functions  $\mathbf{B}$ ,  $T$ ,  $\rho$ ,  $\mathcal{P}$ ,  $\mathbf{v}$  and the dimensionless electric current  $[j]$ , has the form

$$\rho \left( \frac{\partial \mathbf{v}}{\partial t} + (\mathbf{v} \cdot \nabla) \mathbf{v} \right) = -\nabla \left( \mathcal{P} + \frac{B^2}{2} \right) + M \Delta \mathbf{v}, \quad (5)$$

$$\frac{\partial \rho}{\partial t} + \nabla \cdot (\rho \mathbf{v}) = 0, \quad (6)$$

$$\mathcal{P} = \frac{\beta_{0*}}{2} \rho T, \quad (7)$$

$$\frac{\partial \mathbf{B}}{\partial t} = \nabla \times (\mathbf{v} \times \mathbf{B}) - \nabla \times (\Theta \mathbf{j}), \quad \mathbf{j} = \nabla \times \mathbf{B}; \quad (8)$$

$$\begin{aligned} \frac{\beta_{0*}}{2(\gamma-1)} \rho \left( \frac{\partial T}{\partial t} + (\mathbf{v} \cdot \nabla) T \right) + \mathcal{P} \nabla \cdot \mathbf{v} = \\ \nabla \cdot (K \nabla T) + \Theta j^2. \end{aligned} \quad (9)$$

Here,  $\gamma = 5/3$ ; the functions

$$\Theta = \theta_* \beta_{0*}^{1/2} T^{-3/2}, \quad (10)$$

$$K = \kappa_* \beta_{0*}^{3/2} T^{5/2}, \quad (11)$$

$$M = \mu_* \beta_{0*}^{1/2} \quad (12)$$

are, respectively, the local magnetic diffusivity, dimensionless local thermal conductivity and dimensionless kinematic viscosity coefficient (assumed to be independent of the local temperature variations); the dimensionless factors  $\theta_*$ ,  $\kappa_*$ ,  $\mu_*$  do not depend on  $\beta_{0*}$ , being determined in Appendix A by the originally specified dimensional parameters of the medium – specifically,  $\theta_*$  depends on  $T_*$ , and both  $\kappa_*$  and  $\mu_*$  depend on  $T_*$  and  $N_*$ .<sup>3</sup> We do not take into account thermoelectricity and neglect the influence of gas-dynamic viscosity on plasma heating. As already noted, the term taking into account the effect of gravity is omitted in Equation (5). The equation  $\nabla \cdot \mathbf{B} = 0$  is automatically satisfied for the assumed two-dimensional geometry.

We will consider here the dependence of the variables on two spatial coordinates in a plane perpendicular to  $\mathbf{B}$ , in which we introduce a Cartesian coordinate system  $(x, z)$  with the  $x$ -axis directed vertically downward. The distribution of  $B(x, z)$  over the plane is displayed as a greyscale map; we note that, in the geometry considered, the contours of the magnetic-field strength coincide with the electric-current lines.

### 3.2. Initial Conditions

Let the absolute value of the initial magnetic field be symmetric with respect to two symmetry axes,  $x = x_c = x_{\max}/2$  [where  $B(x_c, z)|_{t=0} = 0$ ] and  $z =$

---

<sup>3</sup>In their Sections 2.3 and 2.4, Brushlinskii and Morozov (1980) use the system of Equations (5)–(9) to investigate the plasma and magnetic-field dynamics without taking into account the Hall effect. Thus, this system describes an isotropically conducting plasma. If, however, this effect is included, the system should be supplemented with terms with a parameter  $\xi$  defined by Equation (1) and characterising the difference between the macroscopic (dimensionless) velocities of the ion and electron gases,  $\mathbf{v}_i - \mathbf{v}_e = \xi \mathbf{j} / \rho$ ; see Sections 1.2 and 2.5 of Brushlinskii and Morozov (1980). The presence of these terms implies a tensor form of the transport coefficients, which is equivalent to the appearance of the  $\xi$ -dependent Hall and Pedersen conductivities,  $\sigma_H$  and  $\sigma_P$ . Some important phenomena discovered by Brushlinskii and Morozov (1980) could be accounted for in terms of the local variations of  $\sigma_H$  and  $\sigma_P$  in the course of the plasma and magnetic-field coevolution (Morozov and Solov'ev, 1980; Alekseeva, 1980).



$z_c = z_{\max}/2$ . The distribution of  $B(x, z)|_{t=0}$  is shown in Figure 1a, where the following notation is used:

$$X = (x - x_c)/x_{\max}, \quad Z = (z - z_c)/z_{\max}. \quad (13)$$

An analytic formula that specifies the initial magnetic field  $[B(x, z)|_{t=0}]$  shown in Figure 1a is given in Appendix B. The initial field thus chosen is the sum of two terms (see Appendix B): the first term is smaller in absolute magnitude and is distributed over the light grey and dark grey areas in Figure 1a; the second one is greater and more localised (narrow black and white strips in the figure). Since the equation  $\nabla \cdot \mathbf{B} = 0$  is automatically satisfied in the two-dimensional geometry of the problem, each of these terms can be considered a separate magnetic field, either a distributed or a more localised one.

We assume that the plasma is initially motionless and isothermal:

$$\mathbf{v}(x, z)|_{t=0} = 0, \quad T(x, z)|_{t=0} = 1. \quad (14)$$

In this case, according to Equation (7), the density at  $t = 0$  differs from the pressure only by a constant factor. The initial condition for the pressure should specify, however, the degree of balance between the initial distributions of the magnetic and gas pressure. Here, as in Alekseeva and Kshevetskii (2011), we restrict ourselves to two cases.

*The case of no initial balance (NIB).* If the pressure of the initially specified magnetic field  $B(x, z)|_{t=0}$  is not balanced by the gas pressure, then, according to our choice of units,

$$\rho(x, z)|_{t=0} = 1 \quad (15)$$

and, accordingly, in view of the Equation (7) of state,

$$\mathcal{P}(x, z)|_{t=0} = \beta_{0*}/2. \quad (16)$$

*The case of partial initial balance (PIB).* We assume that, in the case of PIB, the distributed magnetic field, being in balance with the local gas pressure  $\mathcal{P}(x, z)|_{t=0}$ , is superposed with an unbalanced localised magnetic field and the balance thus appears to be only partial. Physically, this case can be interpreted as the penetration of a new, unbalanced magnetic field to the area of the old, pre-existing field (which has already reached a pressure balance). The corresponding formulas for the initial pressure and density are given in Appendix C.

#### 4. The Properties of the Exact Solution Dictated by the Formulation of our Initial-Value Problem.

Our analyses of the form of Equations (5)–(9) with initial conditions given by Equations (14), (25) together with either Equations (15), (16) or (29), (30), lead to the following conclusions.

i) If the initial magnetic and gas pressures are completely balanced, a stationary solution exists. However, in both the cases of a partial balance (PIB) and of

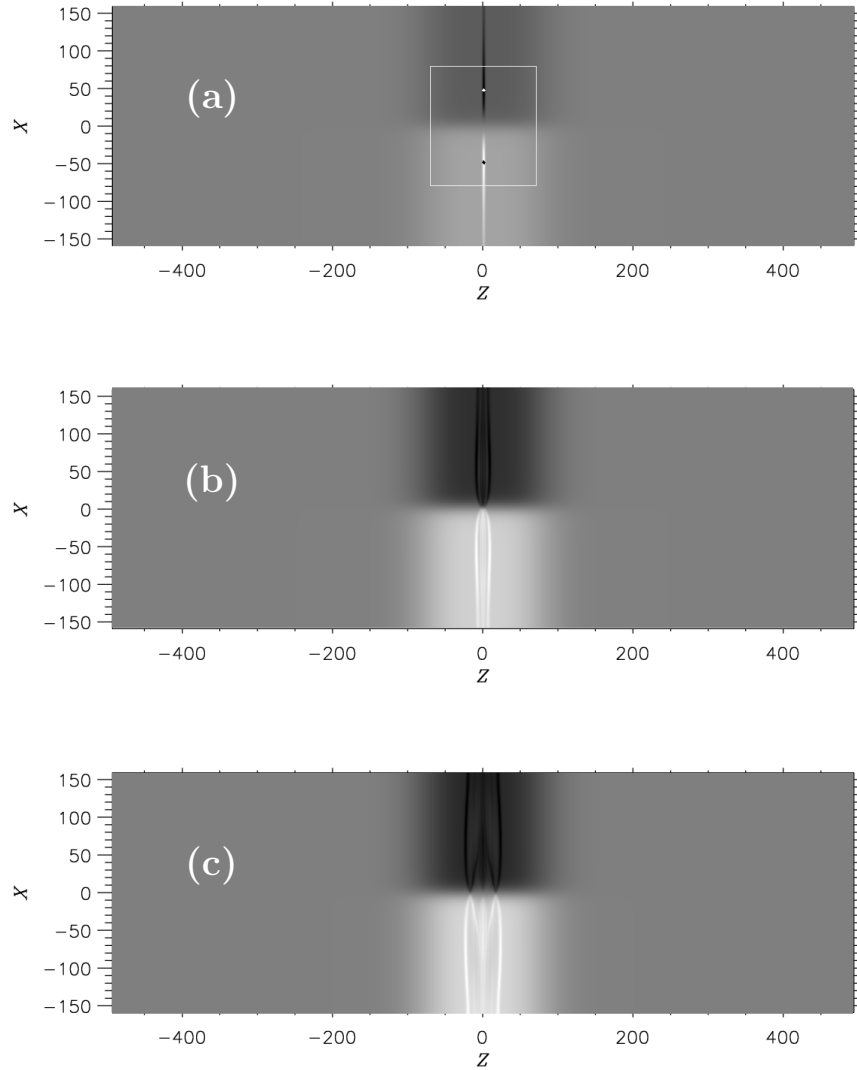


**Figure 1.** Distribution of  $B(x, z)$  in the plane  $(x, z)$  for the outset stage of the magnetic field – plasma coevolution at  $\beta_{0*} = 1.5$  in the absence of gas-dynamic viscosity at different times: (a)  $t = 0$ , the cases of both PIB and NIB (see below in this section); (b)  $t = 0.008$  and (c)  $t = 0.024$ , the case of PIB. The  $x$ -axis is directed downward from the upper left corner, and the  $z$ -axis is directed to the right. The quantities  $X$  and  $Z$  are related to  $x$  and  $z$  according to Equations (13). The image is stretched vertically by a factor of 4.4. Light: positive magnetic field (directed inward); dark: negative magnetic field. The white dot on the dark background and the black dot on the light background mark the positions of the minimum and maximum  $B(x, z)|_{t=0}$ , respectively. [The other greyscale maps represent the central part of this domain, marked with the white frame in panel (a).]

no initial balance (NIB), dynamical processes manifest themselves. We discuss them now assuming that  $M = 0$  in Equation (5).

ii) If the initial configuration of the magnetic field has the form of Equation (25), illustrated in Figure 1a, the subsequent evolution of the magnetic field and plasma state should be similar to those in a laboratory Z-pinch. Note, however, that the contraction of the electric current to the axis  $x = x_c$  does not result here in substantial increases in the maximum  $|\mathbf{B}|$  in view of the planar geometry.

iii) In the NIB case, the coevolution of the plasma and  $\mathbf{B}$  begins with the origin of a system of powerful waves, fast electric-current contraction, collapse of the plasma and its subsequent retreat. All of these processes strongly affect the bulk of plasma.

iv) In the PIB case, the early evolution is more quiet. The unbalanced magnetic-field component  $d$  present between the layers of the balanced field (Figure 1a) form “tongues” stretching to  $x = x_c$ , which provoke the sausage instability. Since  $\mathbf{B} = 0$  at  $x = x_c$ , an  $x$  component of the magnetic-pressure gradient is present near this axis; according to Equation (5), oppositely directed flows with a velocity  $v_x$ , directed toward this axis from the both sides, develop. The form of Equation (8) indicates that the magnetic field is partially frozen in the plasma. Therefore, these flows carry the magnetic field closer to the axis, which results in a further steepening of the magnetic-field gradients, and so they intensify themselves. The substance can freely flow out along the neutral line and then spread from it (no electrodes or walls are present, in contrast to the conditions of laboratory setups). As to magnetic viscosity  $[\Theta]$ , it is not effective damper of the process, since the great gradients of  $B$  correspond to great  $j$ , i.e. enhanced heating of plasma and decreasing of  $\Theta$  in accordance with Equations (9, 11). Therefore, in the absence of gas viscosity  $M$ , the initial-value problem of Equations (5)–(9), (14), (25), (15), (16), or (29, 30) has solutions with the velocity  $[v]$  approaching  $\infty$  with  $t$ . The velocity increases the faster, the closer the magnetic “tongues” to the axis  $x = x_c$ . It is difficult to predict whether this process will be monotonic or impulsive.

v) The most important feature of the process considered is the presence of opposite plasma flows  $[v_x]$  approaching each other through the zone where  $B \approx 0$ . It is therefore reasonable to conjecture that the inclusion of the gas viscosity  $[M]$  in Equation (5) can slow down or even stop the process. (In contrast to the magnetic viscosity  $[\Theta]$ , the gas viscosity increases with temperature according to Equation (23)). Here, we are interested in a qualitative evaluation of the role of the gas viscosity and ignore, for simplicity, its local variations with temperature.

## 5. The Procedure of Numerical Solution

The verification criterion for a numerical code solving the two-dimensional initial-value problem in Equations (5)–(9), (14), (25), (15), (16), or (29, 30) is the similarity between the numerical and exact solutions. However, the numerical solution possesses some features that are not present in the exact solution. For example, the exact solution of the problem in Equations (5)–(9), (14), (25), (15),

(16), or (29, 30) must be of the type of symmetry relative to the axis  $x = x_c$  considered and cannot describe the wriggle (or kink) instability of the Z-pinch, whereas its numerical solution can; the reason is that numerical noise prevents accurately describing the symmetry imposed by the initial conditions.

To solve our initial-value problem numerically, we use a finite-difference scheme that approximates the equations with the second order of accuracy in time and space; central differences are used to approximate the spatial derivatives. It is known that stable numerical methods of second-order accuracy introduce no spurious dissipation (although they may introduce spurious dispersion; methods of a first-order accuracy introduce spurious dissipation without spurious dispersion – see LeVeque, 1992); on this basis, many numerical algorithms free of spurious dissipation have been developed (Thomas and Roe, 1993). Our second-order-accuracy technique belongs to this class of methods free of numerical dissipation.

Our scheme is constructed so as to ensure the existence of a non-increasing grid analogue of the wave-energy functional; this immediately proves a stability theorem for the method. The scheme is conservative, i.e. the energy, mass and momentum are conserved. As already noted, the solution of the problem can be sought in the class of generalised functions; the algorithm is able to automatically make transitions from smooth to generalised solutions and vice versa. Therefore, the method makes it possible to obtain non-differentiable solutions, in particular, with discontinuities (even multiple). This property of our numerical method proves to be important, since we will study the breakdown of the initially smooth field into small-scale waves and other structures, i.e. into the features that can be described either by functions with large derivatives or even by non-smooth functions. Our numerical method generalises the previously developed method for the numerical integration of equations of motion of the atmospheric gas (Kshevetskii and Gavrilov, 2005). Structurally, the numerical-integration formulas resemble those of the Lax–Wendroff method. A comprehensive analysis of our numerical technique was given by Kshevetskii (2006).

Our simulations are carried out under the assumption that the velocity component normal to the boundary of the computation domain and the normal derivative of the magnetic field vanish at this boundary. The computation domain is chosen to be large enough to eliminate boundary effects affecting the processes in its central part, where the phenomena under study develop.

We solve the problem for a chromospheric layer where the temperature of both the ion (proton) and electron components of the plasma is 25,000 K, which gives a total characteristic temperature of  $T_* = 50,000$  K for the plasma medium. We assume here  $N_* = 10^{15} \text{ m}^{-3}$  (Demoulin and Klein, 2000). In such a layer,  $\theta_* = 1.2 \times 10^{-8}$ ,  $\kappa_* = 3.8 \times 10^{-4}$ , and  $\mu_* = 5 \times 10^{-6}$  (see Appendix A).

Further, we consider the case of  $\beta_{0*} = 1.6$  turning sometimes to those of  $\beta_{0*} = 1.5$  or  $\beta_{0*} = 2.3$ . In accordance with Section 3, the dimensional units for the case of  $\beta_{0*} = 1.6$  are:  $B_0 = 0.33$  G,

$$v_{0*} = 23 \text{ km s}^{-1}, \quad t_{0*} = 1.1 \text{ minutes.} \quad (17)$$

The applicability of the our initial-value problem to description of plasma dynamics at this intensity of  $B_0$  is discussed in Appendix D.

The calculations for  $M = 0$  were carried out in a domain with  $x_{\max} = 0.207$ ,  $z_{\max} = 2.8$ , which corresponds to 300 km (320 grid points) in height and 4200 km (988 grid points) in the horizontal direction. For  $M \neq 0$ , the domain measures  $0.207 \times 0.639$ , or  $300 \times 922$  km<sup>2</sup>, with  $80 \times 247$  grid points.

## 6. Results

### 6.1. The Phenomenon of Velocity Burst

Our simulations reveal an ensemble of primary waves produced by contraction and expansion of the whole current zone associated with the unbalanced component of  $\mathbf{B}$  (see Section 2.2 and Figures 1b,c). Against the background of these waves, at the centre of the magnetic configuration, the pinch-sausage instability begins developing and becomes especially pronounced after the waves leave this area (see Section 7).

As shown previously (Alekseeva and Kshevetskii, 2011), the nonlinear stage of the pinch-sausage instability forms cross-shaped transient structures, which are more complex and smaller in size in the calmer PIB case, as compared with the more dynamical, completely unbalanced NIB case. The development of the pinch-sausage instability in the PIB case passes through two early stages: only after this pinch effect has manifested itself in the unbalanced component of the magnetic field and has produced its cross-shaped pattern, does the sausage instability set in in the balanced component of the field, and the concentration of the whole magnetic field approaches the symmetry axis  $x = x_c$  of the initial magnetic configuration. This gives rise to intricate transient flow structures, which facilitate the development of turbulence and, accordingly, favour the heating of the plasma. Thus,  $T$  can be observed to double in the PIB case, while no appreciable temperature changes are associated with the pinch instability in the NIB case.

Now, simulations based on the improved algorithm ensuring higher accuracy reveal another peculiarity of the coevolution of the magnetic field and plasma state in the PIB case (Figure 2). Against the background of the above-mentioned fairly gradual variations in the physical quantities, impulsive phenomena of increasing plasma velocity, i.e. velocity burst, develop, no similar phenomena being observed in the case of NIB.

The numerical result obtained here agrees with the properties of the exact solution deducible from the mathematical form of our initial-value problem (see Section 4). Thus, in the PIB case, we observe the whole scenario of the sausage pinch instability, up to the manifestation of the final velocity burst. (We note that no exceptions occur in the process of computation, and the code continues running with progressively decreasing steps).

Generally,  $\beta_{0*}$  is higher, the slower the process (Figure 2); we also observe this regularity in other numerical simulations, not described here, although there is no smooth dependence of the parameter values  $\beta_{0*}$  (see Figures 2a,b for an example).

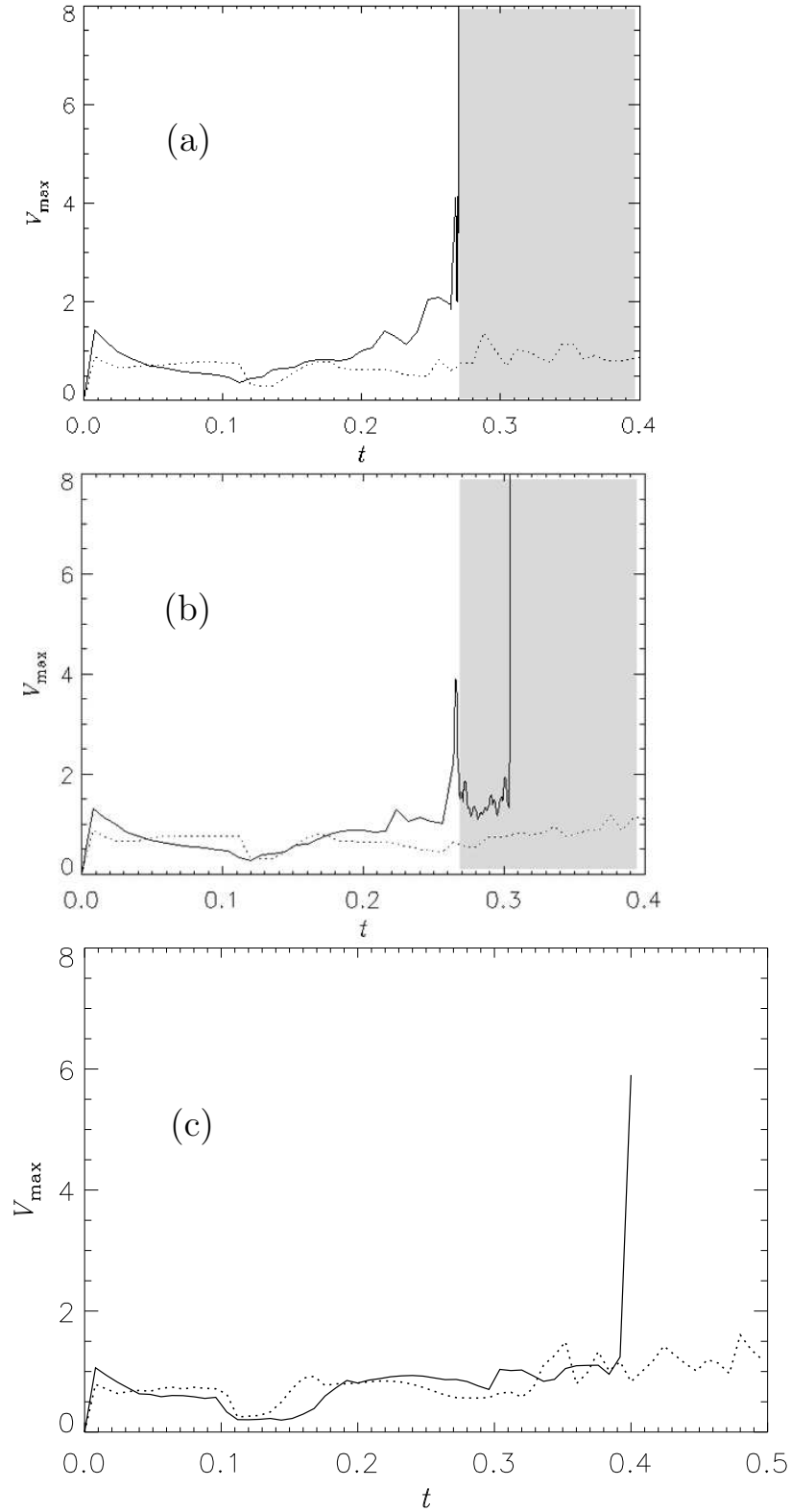


**Figure 2.** The maximum absolute velocity over the computation domain as a function of time in the cases of PIB (solid curve) and NIB (dotted curve) at  $\beta_{0*} = 1.5$  (a),  $\beta_{0*} = 1.6$  (b) and  $\beta_{0*} = 2.3$  (c) in the absence of gas viscosity  $[M]$ .

Physical reasons for this effect can naturally be expected, since we solve an initial-value MHD problem with an unstable initial magnetic configuration, where the sausage instability develops under different physical conditions due to the presence of interfering primary waves, even at very close values of  $\beta_{0*}$  (see Section 7.1 below).

Also, no smooth transition between the final stage of the numerical solutions should be expected since the required accuracy can more hardly be achieved. For example, in both cases  $\beta_{0*} = 1.5$  and  $1.6$ , our numerical solutions represent the evolution of the process with the gradual velocity variations changing into a dramatic increase (the white areas in Figures 2a,b). This increase should result in a rapid growth of both physical and numerical instabilities with the spatial scale of disturbances approaching zero. At this stage (the shaded areas in Figures 2a,b right of about  $t = 0.27$ ), the simulation requires progressively shorter time steps and catastrophically loses its accuracy. Thus, the white and shaded areas correspond to a normal and a poor accuracy, respectively (this is why the small change in  $\beta_{0*}$  can delay the final infinite velocity growth). However, we do show the curves in the shadowed areas in Figures 2a,b, since they demonstrate that our numerical solution actually reproduces the analytically predicted velocity divergence. In no way does it give a quantitative description of the final stage of the processes.

## 6.2. Velocity Burst and the Known Pinch-Effect Features

We consider the process in more detail precisely for the case  $\beta_{0*} = 1.6$ , where individual peaks can be singled out. Each of them has features of an underdeveloped final velocity burst. The solution at  $\beta_{0*} = 1.6$  shows that a first, faint velocity burst with a peak velocity of  $v_1 = 1.2$  at  $t = 0.224$  precedes the second one with  $v_2 = 3.9$  at  $t = 0.266$  (Figure 2). The first burst appears when the cross-shaped pattern has already formed (Figure 3).

Later, the distributed magnetic field approaches the symmetry axis  $x = x_c$  to occupy an area initially free of magnetic field (Figure 4, left). This induces a sharp increase in the current-aligned velocity (which is seen as a brightening along the axis  $x = x_c$  in Figure 4, right). The high-speed jets corresponding to the peak of the velocity burst are located in the central part of the magnetic configuration (Figure 5). This velocity burst occurs in a time interval of duration 0.0028.

Since the plasma velocity  $\mathbf{v}$  in the system of MHD equations (Brushlinskii and Morozov, 1980) coincides with the bulk velocity of the ion component  $\mathbf{v}_i$ , at the velocity burst, an ion acquires an additional kinetic energy of  $m_i v^2/2$ . This corresponds to the ion kinetic temperature  $T_{ki} = 511,000$  K gained rapidly, in 0.1 seconds. Thus, we see that the velocity burst produces suprathermal protons.

In Section 3.1, we assumed that the gravitational acceleration of plasma should not be taken into account in our consideration. Now we can substantiate this assumption knowing that large velocities are achieved (Figure 2). Even in the extreme case of free fall, in a time interval of  $\Delta t \sim 5.3$  seconds, a plasma parcel would gain a velocity increment of  $\Delta v \sim g\Delta t \sim 1.45 \text{ km s}^{-1}$ , which

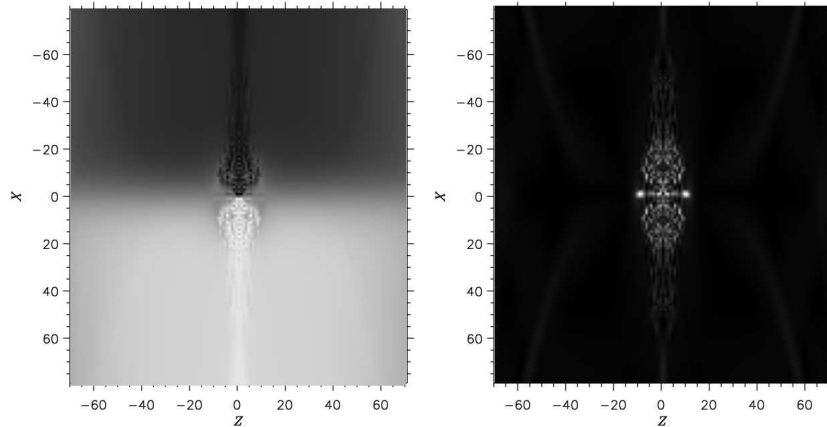


**Figure 3.** Distribution of  $B$  (left) and  $v$  (right) in the plane  $(x, z)$  at  $t = 0.216$ ,  $M = 0$ .

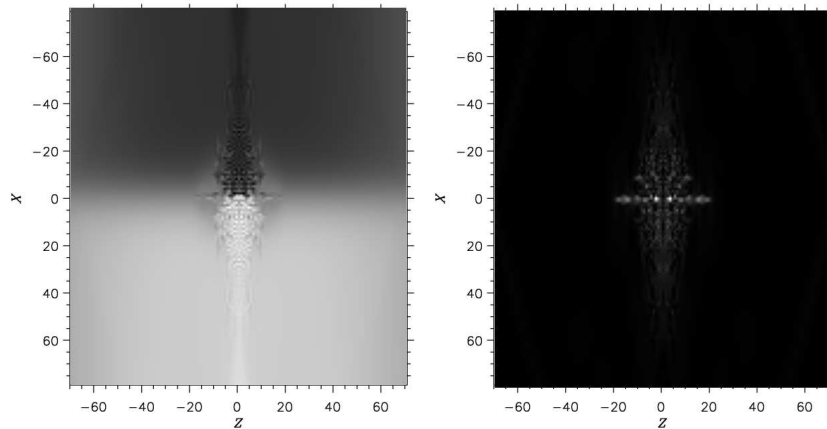


**Figure 4.** Distribution of  $B$  at  $t = 0.256$  (left) and  $v$  at the onset of the velocity burst,  $t = 0.264$ , (right) in the plane  $(x, z)$ .

is vanishingly small compared to the typical plasma velocities, not to mention the burst velocities. (Including this estimate was kindly suggested to us by the referee.)

### 6.3. The Increase of the Magnetic-Pressure Gradient as the Producer of the Velocity Burst

The idea of the physical mechanism of the velocity burst can be formed if we consider the behaviour of other quantities during this burst. Only the region shown in Figure 5, right, will be considered in what follows. The subscripts max and min will refer to maximum and minimum values of a quantity at hand over this very region.

Note that  $B$ ,  $\rho$ ,  $\mathcal{P}$  and  $T$  vary in the burst area not so strongly as  $v$  does (Figure 6). However, according to Equation (5), the velocity variations are directly



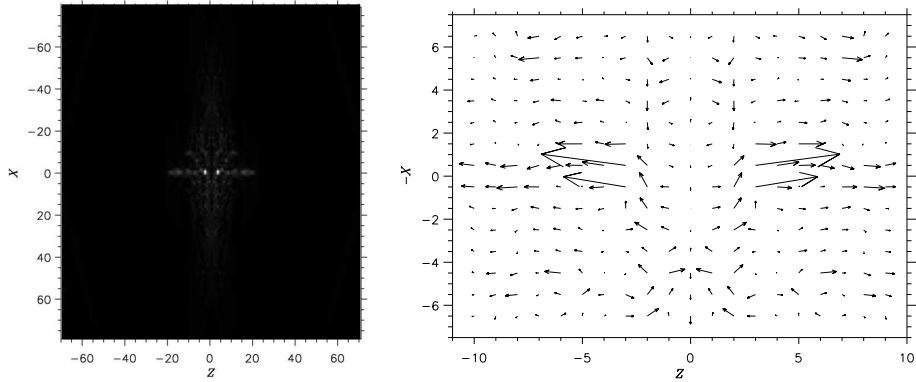


**Figure 5.** Distribution of  $v$  (left) in the plane  $(x, z)$  at the time of the second velocity peak,  $t = 0.2656$ . Right: vector map of  $\mathbf{v}$  (magnified) for the same time. A division of the vertical ( $x$ ) axis is 0.93 km; of the horizontal ( $z$ ) axis, 4.25 km. The longest arrow corresponds to a velocity of  $v_2 = 3.9$ .

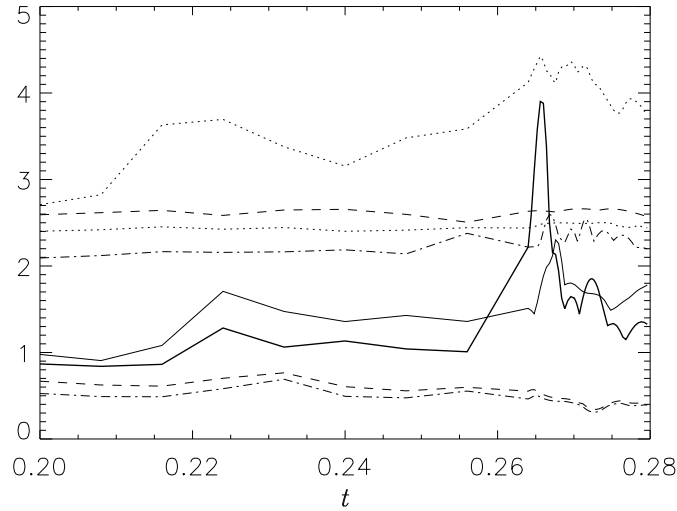


**Figure 6.** Temporal variation of MHD quantities near the time of velocity burst:  $v_{\max}$  (heavy solid curve),  $(B^2/2)_{\max}$  (light solid curve),  $2.5T_{\max}$  (heavy dotted curve),  $2.5T_{\min}$  (light dotted curve),  $2.5\rho_{\max}$  (heavy dashed curve),  $2.5\rho_{\min}$  (light dashed curve),  $2.5\mathcal{P}_{\max}$  (heavy dot-dashed curve),  $2.5\mathcal{P}_{\min}$  (light dot-dashed curve).

controlled by the gradient of the full pressure rather than the above-mentioned quantities. Note that the elevated-gradient areas of the magnetic and the full pressure are virtually coincident (Figure 7), the former giving a dominant contribution to the latter. Consider how the magnetic-pressure gradient is related to the velocity (Figure 8). Indeed, the velocity vector is aligned with the gradient of the magnetic field pressure wherever both are graphically representable, although this is not seen everywhere. However, the gradients cannot always be judged by

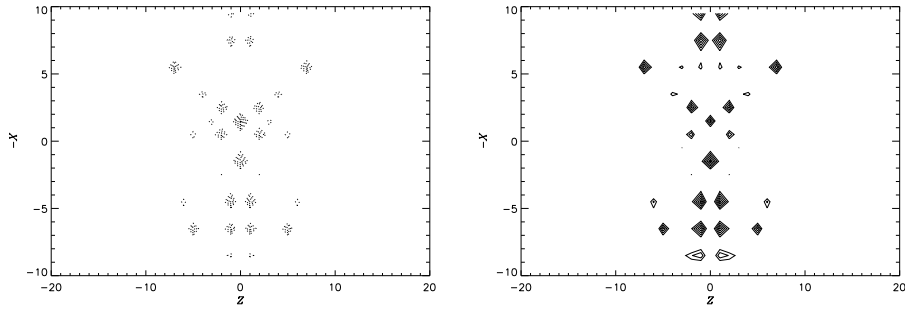


**Figure 7.** Maps of the total pressure (left) and magnetic pressure (right) at an intermediate development stage of the burst ( $t = 0.2648$ ). Areas where the pressure exceeds its mean value over the region are hatched.

the contours plotted; this is all the more so because even large gradients can be handled by our code using generalised functions.

The velocity-burst mechanism could likely be described as follows. In such an impulsive process, the velocity increase achieved over a time interval  $[\delta t]$  is

$$\delta v \approx \delta t \frac{1}{\rho} \left| \nabla \frac{B^2}{2} \right|. \quad (18)$$

Generally,  $|\nabla B^2/2|$  can reach large values, and our technique makes it possible to simulate cases with large gradients.

A link between velocity increases and the presence of large magnetic-field gradients can be revealed by an analysis of temperature variations in the burst area. The temperature is increasing during the burst (Figure 6); this occurs where the density values are reduced and the temperature increase is therefore not an adiabatic effect of gas compression (Figure 9). Actually, the plasma is heated by electric currents, and the temperature is the higher, the larger the current density. In our 2D geometry, the current-density magnitude is proportional to  $|\nabla B|$ . A comparison of the temperature–velocity maps (Figure 10) for the initial stage of the process and for a well-developed burst shows that the longest arrows issue from the areas of increased temperature, i.e. of increased gradients of  $B$ .

The velocity burst revealed here is accompanied by large velocity gradients; therefore, this burst should be affected by viscous forces if  $M \neq 0$  is taken into account in Equation (5). To verify our suggestion that the velocity-burst mechanism stems from Equation (18), we have carried out calculations for the case of  $M \neq 0$  assuming  $\mu_*$  value exaggerated by a factor of 20 compared with the actual viscosity calculated according to Equation (24) for the considered solar-plasma layer. The presence of such a viscosity was even able to suppress the dramatic growth of  $v_{\max}$  at the final development stage of the pinch instability. The evaluation of the specific peak value of  $v_{\max}$  requires taking into account the dependence of viscosity on the local temperature and using an accurate expression for the viscous-stress tensor.

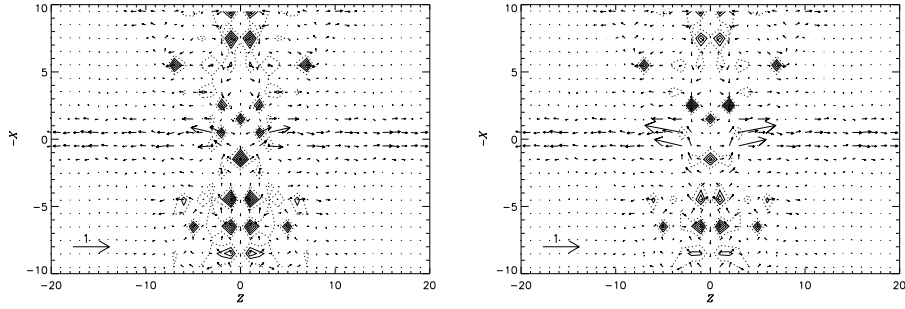


**Figure 8.** Normalised velocity  $v_N$  and contours of the magnetic pressure for an early ( $t = 0.2640$ , left) and the highest ( $t = 0.2656$ , right) development stages of the burst. The dotted curve corresponds to a level of  $(1/3)[(B^2/2)_{\max} - (B^2/2)_{\min}]$ . The unit-length arrow is shown near the lower left corner of each panel; it corresponds to the longest arrow in Figure 5, right.

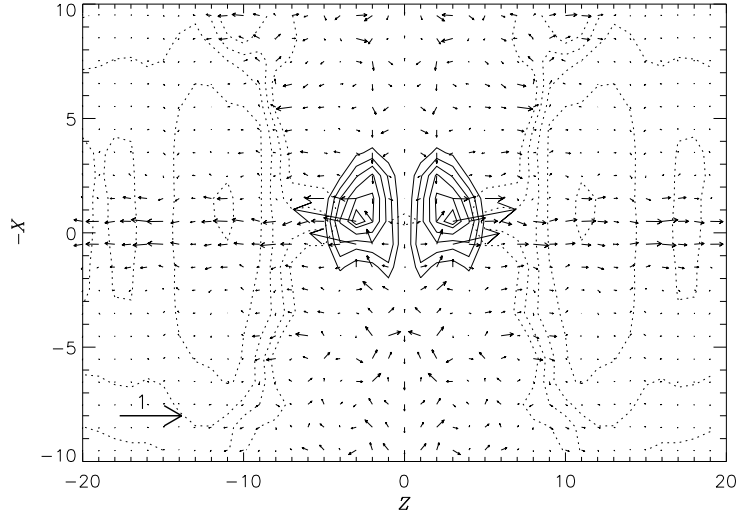


**Figure 9.** Normalised velocity  $v_N$ , temperature  $T$  (solid curves) and density  $\rho$  (dotted curves) for the highest stage of burst development ( $t = 0.2656$ ). Contour levels from 1.456 to the peak value with an increment of 0.076 are used for  $T$ ; from 0.736 with an increment of 0.086, for  $\rho$ . The unit-length arrow is shown near the lower left corner; it corresponds to the longest arrow in Figure 5, right. It can be seen that the temperature reaches its maximum where the density is reduced.

## 7. Discussion

### 7.1. The Onset of the Sausage Instability Against the Background of Interfering Waves

Thus, our numerical simulations reveal a velocity burst, which is observed only at the initial conditions of the PIB type, the case physically corresponding

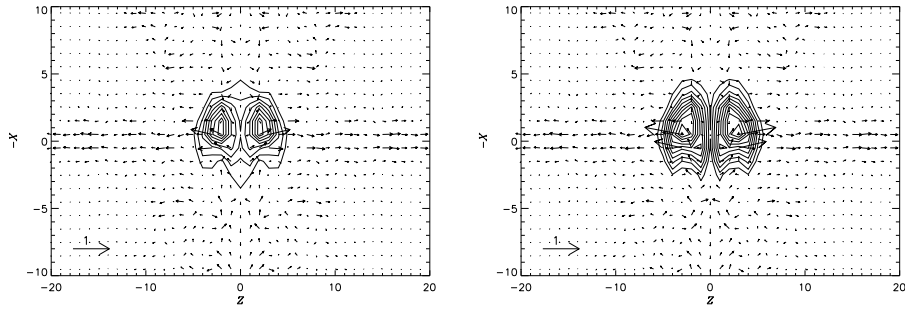


**Figure 10.** Normalised velocity  $v_N$  and temperature for an early ( $t = 0.2640$ , left) and the highest ( $t = 0.2656$ , right) development stages of the burst. The lowest contour level 1.28 and the contour increment 0.048 are the same in both panels. The unit-length arrow is shown near the lower left corner of each panel; it corresponds to the longest arrow in Figure 5, right.

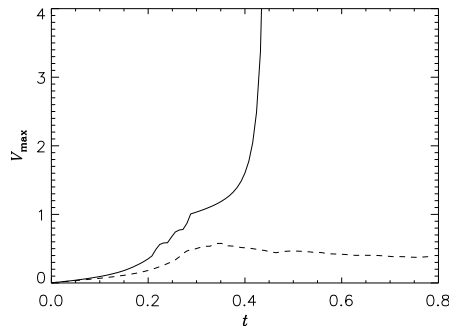


**Figure 11.** The maximum absolute velocity over the computation domain as a function of time in the case of PIB at different viscosity  $\mu_* = 0$  (solid curve) and  $\mu_* = 10^{-4}$  (dashed curve).

to the penetration of a new, unbalanced magnetic field to the area of pre-existing field, which has already reached pressure balance (Section 3.2). This impulsive phenomenon is given by the spontaneously developing sausage instability in the course of the general plasma and magnetic-field evolution (see Section 2.2). At some time, the instability begins developing in the central part of the configuration amidst the primary waves produced by the unbalanced  $\mathbf{B}$  (Figure 12). Ultimately, it leads to the divergence of the solution, which was predicted analytically.

The rate of the instability development should depend on the spatial distribution of the quantities at the onset of instability (as the growth rate of the amplitude depends on the perturbation wavevector in equilibrium configurations according to the linear theory of the sausage instability). Therefore, the particular interference pattern of primary waves at the time of onset should affect the particular scenario of instability development and, eventually, the time of divergence.

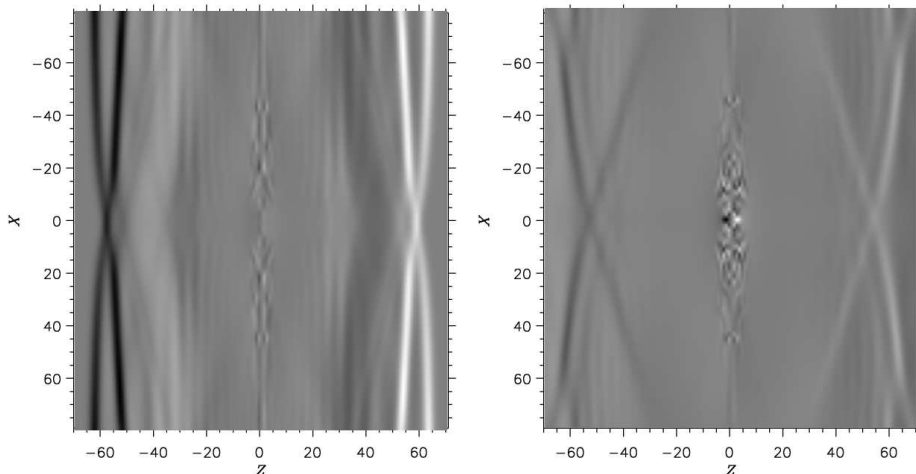


**Figure 12.** The maximum value of the velocity component along the contact zone over the computation domain in the case of PIB  $\beta_{0*} = 1.5$  at  $t = 0.08$  (left) and  $t = 0.136$  (right). The sausage instability starts developing amidst primary waves.

This obvious feature of the solutions should be kept in mind comparing the solutions for close values of the external parameters of the problem, e.g., for  $\beta_{0*} = 1.5$  and  $1.6$  (Figures 2a,b). Although processes of the type ii) giving rise to primary waves (see Section 2.2) differ very little, stronger magnetic fields ensure greater amplitudes and steeper profiles of waves; therefore, the wavevectors of the interference patterns is highly sensitive to the parameter  $\beta_{0*}$  variations. This results in different temporal variations of the maximum velocity seen in the *white* regions of Figures 2a and 2b (note that, at different times, the maximum velocity is generally reached at different points, directly depending on the temporal variation of the interference pattern). At later times, when the disturbance related to the sausage instability becomes strong, the differences in the behaviour of the curves become greater (the *shaded* regions of Figures 2a and 2b). Thus, the manifestations of the velocity burst depend on the fine details of the early development stage of the instability.

## 7.2. Velocity Burst and the Problem of Dynamic Chromospheric Energisation

In our initial-value problem, the plasma is initially motionless and has a constant temperature of 50,000 K throughout the plasma volume. Further, the magnetic-field energy transforms into the thermal and kinetic energy of the plasma because of the development of a pinch with a sausage instability.

For example, in the numerical simulations at  $\beta_{0*} = 1.6$  in the absence of gas viscosity, the plasma temperature increases by a factor of two, whereas the kinetic temperature of the proton component reaches a peak value of 0.511 MK at undimensional  $t = 0.2656$ , or an average particle energy of 44 eV, and substantially exceeds it at later times during the final velocity burst (Figure 2b;

we note that the exact solution goes to infinity – see Section 4). We see that impulsive processes can manifest itself against the background of a gradual development of the pattern. Specifically, intense plasma streams emerge in a temporal interval of about 0.1 second or less near the centre of the magnetic configuration. Such a velocity burst can physically be interpreted as an event of suprathermal-ion generation. This is indicative of the dynamic energisation of a parcel of chromospheric plasma to coronal temperatures and, if the final stage is achieved, of the increase in the kinetic temperature to high values, even those observed in flares.

Note that magnetic reconnection is not present in our solution: it would generate plasma flows varying *along* the magnetic-field line, which is forbidden by the chosen 2D geometry without variations of the physical quantities in the direction of  $\mathbf{B}$ . Therefore, under the conditions of the upper chromosphere, the pinch-sausage effect can be considered a possible alternative to the magnetic-reconnection process as the producer of flares. However, it can develop only in the presence of the “old” magnetic field, which has already reached pressure balance (we recall that, in Figure 2, the curves for PIB case, in contrast to NIB case, demonstrate the velocity burst; see also Appendix C).

To describe the velocity burst more accurately, the equation system used here should be generalised by adding more physical processes. Thus, our simulations suggest that a finite gas viscosity can reduce the kinetic temperature of the fast streams. There are a number of possibilities to obtain more realistic solutions: introducing an adequate gas viscosity in the system of collisional MHD equations; including terms with the Hall-plasma-dynamics parameter  $\xi$ , i.e. considering a conductivity tensor with  $\sigma_H$  and  $\sigma_P$  present; and proceeding to three-dimensional simulations (which, in particular, could make it possible to consider also magnetic reconnection). This work is currently underway.

### 7.3. Velocity Burst and the Ion Beams

The suprathermal ions (protons) revealed in our simulations are related to a phenomenon known from laboratory nuclear-fusion experiments probably. Specifically, neutrons were produced in Z-pinch plasma by relatively small quantities of “beam” deuterium ions accelerated in the direction of the current to energies of 50–200 keV due to the development of the “sausage”  $m = 0$  instability of the pinch. Colliding with the deuterium ions whose temperature was much lower, the beam ions produced fusion neutrons, which were therefore not thermonuclear (Velikovich *et al.*, 2007). The origin of this phenomenon due to the nonlinear evolution of the  $m = 0$  instability of a stagnated compressional Z-pinch is still not fully understood. Some of the proposed mechanisms are fluid-like and others are kinetic in nature. From the MHD standpoint, ion jets in both directions should occur equally from the “necked” region. Presumably, it requires introduction of the Hall term and/or, the finite ion Larmor radius terms in the stress tensor to break this symmetry and allow a beam in the direction of the current to form (Haines, 2011).

Some results of our numerical experiment with MHD hydrogen proton plasma show evidence of their correspondence to this situation. In the PIB case, where

stagnation is initially present, a nonlinear state of the pinch process gives rise to opposite current-aligned ion jets of short duration in the centre of the magnetic configuration (Figures 2 and 5). The energies of ions accelerated during the final velocity burst would be comparable with the energy value indicated above for the deuterium ions obtained in laboratories. It is worth adding that the simulated pair of suprathermal-ion jets could actually produce an ion beam accelerated in the direction of the current. Indeed, suprathermal ions experience less frequent collisions than the thermal particles of the plasma and are more directly controlled by the electromagnetic field. Near the symmetry axis along which they move, the magnetic field is weak. The electric field should accelerate the ions of one jet and decelerate the ions of the oppositely directed jet. Therefore, only one ion beam will be produced.

## 8. Conclusion

Contacted oppositely directed horizontal magnetic fields are not rare in the upper chromosphere, where the plasma is fully ionised. Therefore, the phenomena described by our numerical solutions should not be unusual.

We have traced the coevolution of the plasma and magnetic field from the origin of the steadying waves to the final stage when a velocity burst occurs. The temperature of the chromospheric plasma increases by two to three times in the course of the evolution. The velocity burst is due to the sausage instability that develops against the background of the steadying waves, turbulence, frontal zones, *etc.* As a result, fast streams suddenly appear at the centre of the magnetic configuration. The kinetic temperature corresponding to such fast streams can approach the values recorded in the corona and, likely, in flares. So, the pinch-sausage effect can be a possible energiser of the upper chromosphere and an alternative to the magnetic-reconnection process in producing flares.

We have numerically solved the standard self-consistent MHD system of equations. This made it possible to relate the plasma–magnetic–field coevolution to the initial values of the basic MHD quantities without invoking ad-hoc non-observable parameters. The standard form of the MHD system allows us to compare our results for the solar plasma with those for the laboratory plasma, and we note that the velocity burst revealed in our simulations resembles the sudden emergence of high-speed proton beams in laboratory Z-pinch devices.

## Appendix

### A. Material Properties of the Medium

*Magnetic diffusivity.* Following Spitzer (1962) and Priest (1982), we define the conductivity  $[\sigma]$  of a collisional, fully ionised hydrogen plasma as

$$\sigma = \frac{e^2 N_e \tau_e}{m_e}, \quad (19)$$

where  $N_e$  and  $\tau_e$  are the local electron concentration and electron–ion collision time. In a fully ionised gas there is some uncertainty as to the appropriate value of  $\tau_e$  to use in this equation (Spitzer, 1962). We choose  $\tau_e$  in accordance with formula (2.5e) of Braginskii (1965), which coincides with  $\tau_e$  in § 5.7 of Balescu (1988). [Thus, our  $\sigma$  is equal to that used by Brushlinskii and Morozov (1980) and Brushlinsky (1989). It is also used as a basis for the generalisation of the form of conductivity to the case of plasma with neutral particles (Leake and Arber, 2006).] Explicitly writing  $\tau_e$  yields  $\Theta$  in the form Equation (10), where

$$\theta_* = \sqrt{\frac{m_e m_i c^2}{2\pi} \frac{1}{H} \frac{\Lambda e^2}{(kT_*)^2 0.75}} \quad (20)$$

( $\Lambda$  is the Coulomb logarithm, which we set here equal to 20).

In a quasi-neutral plasma,  $\sigma \propto N_e \tau_e$  is a function of only the local temperature.

*Thermal conductivity and gas-dynamic viscosity coefficient.*

The thermal conductivity of a collisional plasma differs substantially between the region of magnetised plasma and the region of zero magnetic field. In the (dimensional) heat-transfer equation (Braginskii, 1965), we use the quantity corresponding to the case of weakly magnetised plasma (where, in the commonly accepted notation,  $\kappa_{\perp} \sim \kappa_{\perp}^e \sim \kappa_{\parallel}^e$ ). Once the nondimensionalisation of the equations is accomplished, this coefficient, appearing in the expression for Equation (11), determines

$$\kappa_* = \frac{k_s T_*^2 \sqrt{m_i}}{32 H k^{3/2} N_*}, \quad (21)$$

$$k_s = \frac{3.16 \cdot 0.75}{\Lambda \sqrt{2\pi}} \frac{k^{7/2}}{\sqrt{m_e} \cdot e^4}, \quad (22)$$

(note that the so-called Spitzer thermal conductivity [ $k_s$ ] has dimensions of  $\text{erg s}^{-1} \text{cm}^{-1} \text{deg}^{-7/2}$ ). This substantially overstates the thermal conductivity in the region of the strong magnetic field; however, as our results indicate (Alekseeva and Kshevetskii, 2011), major thermal changes occur in the region of weak magnetic field  $x = x_c$ .

The expression for the kinematic-viscosity coefficient of plasma with a magnetic field is very complicated (Braginskii, 1965). Instead, even in the case of a magnetic field present, Priest (1982) and Spitzer (1962) consider the coefficient of plasma without magnetic field

$$M_0 = 2.21 \times 10^{-15} \Lambda^{-1} (T_i/\text{K})^{5/2} \text{g} \cdot \text{cm}^{-1} \cdot \text{s}^{-1}, \quad (23)$$

where  $T_i$  is the ion temperature in K (since the gas-dynamic viscosity of plasma is determined by ions, it is worth recalling that the ion temperature is half the plasma temperature under consideration). That practice is appropriate for use in our investigation, since, in the magnetic fields studied with the pinch effect, the most interesting phenomena arise in the neighbourhood of the neutral line



where magnetic field is not great. So we obtain  $M$  in Equation (12) with the dimensionless parameter  $[\mu_*]$  determined by

$$\mu_* = \frac{0.215}{\Lambda} \frac{T_*/(1 \text{ K})}{N_* \times (1 \text{ cm}^3)}. \quad (24)$$

The present study addresses the qualitative role of viscosity; therefore, the simplest form of the viscous force is used in Equation (5).

## B. Initial Magnetic-Field Distribution

The structure of the magnetic field at the initial time is determined by the expression

$$B(x, z)|_{t=0} = D(x, z) + d(x, z), \quad (25)$$

$$D = [1 + \zeta \exp(-\zeta)] \tanh[q(x - x_c)], \quad \zeta \equiv (z - z_c)^2/z_k^2, \quad (26)$$

$$d = D \frac{s(x - x_c)^2 \exp(-1000\zeta)}{[x_s^2 + (x - x_c)^2]^2 [1 + s_1(z - z_c)^2]}, \quad (27)$$

where  $q = 130$ ,  $x_s = 0.031$ ,  $x_c = x_{\max}/2$ ,  $z_c = z_{\max}/2$ .

Plasma with zero gas-dynamic viscosity was simulated in a computational domain with  $x_{\max} = 0.207$ ,  $z_{\max} = 2.8$  at  $s_1 = 1.76$ ,  $z_k = 0.17$ ,  $s = 0.01$ . With this choice of constants, the term  $|D|$  in Equation (25) is approximately half of the value of  $|d|$ . For a viscous plasma, the calculations were carried out in a computational domain with  $x_{\max} = 0.207$  and  $z_{\max} = 0.639$  at  $s_1 = 0$ ,  $z_k = 0.025$ ,  $s = 0.00025$ . Therefore, we get  $|D| \approx |d|$ .

## C. Initial Pressure and Density in the PIB Case

Recall that  $\rho(x, z)|_{t=0} = 1$  outside the region occupied by the magnetic field. Assume that, in the region of the magnetic field Equation (25), only the component  $D$  is in equilibrium with the gas pressure:

$$\mathcal{P}(x, z)|_{t=0} + D(x, z)^2/2 = \beta_{0*}/2. \quad (28)$$

Taking into account Equation (7) leads to the following initial conditions for pressure and density:

$$\mathcal{P}(x, z)|_{t=0} = \beta_{0*}/2 - D(x, z)^2/2, \quad (29)$$

$$\rho|_{t=0} = 1 - \frac{D(x, z)^2}{\beta_{0*}}. \quad (30)$$

## D. The Applicability of the Considered Initial-Value Problem to the Case of $\beta_{0*} = 1.5 - 2.3$

Weak magnetic field evolves slowly and requires computations over long periods to reach the divergence of the solution (described in Section 4). This leads to accumulation of errors. Therefore, we choose the characteristic  $B$  value to be as large as  $B_0 = 0.33$  G.

Although this  $B_0$  corresponds to characteristic values  $\omega_{e0}\tau_{e*} \gg 1$ , we nevertheless use it to solve numerically the initial-value problem – Equations (5) – (9), (14), (25) and either (15), (16) or (29), (30) – with isotropic  $\Theta, K, M$ , intending to supplement the system, at a later time, with terms including the parameter  $\xi$ , or, in other words, to automatically take into account the anisotropy of the local coefficients in the areas where this anisotropy is substantial (see footnote in Section 3).

However, in the magnetic configuration considered (Figure 1a), the most important phenomena develop near the line of contact of opposite polarities  $x = x_c$ , where magnetic field vanishes and the local coefficients are therefore isotropic (see Section 4). Thus, the results obtained for the given  $B_0$  appear to adequately reflect the reality. (We can also note that our tentative calculations with  $\xi \neq 0$  for the same magnetic configuration and initial conditions show virtually no difference with the case of  $\xi = 0$  presented here; only a more rapid evolution is observed.)

**Acknowledgments** We cordially thank A.V. Getling for carefully considering the ideas of this study and useful recommendations. We are also grateful to the referee for discussions. This work was supported by the Russian Foundation for Basic Research (project no. 12-02-00792-a).

## Disclosure of Potential Conflicts of Interest

The authors declare that they have no conflicts of interest.

## References

- Alekseeva, L.M.: 1980, Physical nature of the anode explosion in plasma channels. *Sov. Tech. Phys. Lett.* **6**(11).
- Alekseeva, L.M.: 1997a, Generation of magnetic field by acceleration of Hall plasma and some consequences of this process. In: Bordage, M.C., Gleizes, A. (eds.) *XXIII Internat. Conf. on Phenomena in Ionized Gases 2*, Université Paul Sabatier, Toulouse, 156.
- Alekseeva, L.M.: 1997b, Hall effect as a producer of effective gravity and of quasi-acoustic-gravity waves in plasma flows. In: Bordage, M.C., Gleizes, A. (eds.) *XXIII Internat. Conf. on Phenomena in Ionized Gases 1*, Université Paul Sabatier, Toulouse, 206.
- Alekseeva, L.M.: 1999, Effective gravity due to the Hall effect and quasi-acoustic-gravity waves in accelerated plasma flows. *J. Plasma Phys.* **61**, 671. DOI. ADS.
- Alekseeva, L.M.: 2006, The Hall effect as the producer of current sheets in astrophysical plasmas. *Astron. Lett.* **32**, 274. DOI. ADS.
- Alekseeva, L.M., Kshevetskii, S.P.: 2006, Numerical simulations of the MHD structuring of rarefied solar plasma. In: *Multiwavelength Investigations of the Sun and Modern Problems of Solar Activity*, All-Russia Conference, Abstracts, Special Astrophysical Observatory, Russian Academy Sci., 12.

- Alekseeva, L.M., Kshevetskii, S.P.: 2011, Solar plasma structuring due to two-dimensional pinch effect over the photosphere. *Astrophys. Bull.* **66**(1), 72.
- Alekseeva, L.M., Solov'ev, L.S.: 1964, Current vortices and critical surfaces in a magnetohydrodynamic flow. *Prikladnaya Matematika i Mekhanika* **28**(6), 987.
- Aschwanden, M.J.: 2001, An evaluation of coronal heating models for active regions based on Yohkoh, SOHO, and TRACE observations. *Astrophys. J.* **560**, 1035. DOI. ADS.
- Aschwanden, M.J.: 2004, *Physics of the Solar Corona. An Introduction*, Springer, Berlin.
- Aschwanden, M.J.: 2008, An observational test that disproves coronal nanoflare heating models. *Astrophys. J. Lett.* **672**, L135. DOI. ADS.
- Aschwanden, M.J., Nightingale, R.W.: 2005, Elementary loop structures in the solar corona analyzed from TRACE triple-filter images. *Astrophys. J.* **633**, 499. DOI. ADS.
- Balescu, R.: 1988, *Transport Processes in Plasmas* **1**, Elsevier, Amsterdam.
- Braginskii, S.I.: 1965, Transport processes in a plasma. In: Leontovich, M.A. (ed.) *Rev. Plasma Phys.* **1**, Consultants Bureau, New York, 205.
- Brushlinskii, K.V., Morozov, A.I.: 1980, Calculation of two-dimensional plasma flows in channels. In: Leontovich, M.A. (ed.) *Rev. Plasma Phys.* **8**, Consultants Bureau, New York, 105. ADS.
- Brushlinskii, K.V., Gerlakh, N.I., Morozov, A.I.: 1968, Two-dimensional steady flow of highly conducting plasma in a coaxial system. *Fluid Dynamics* **1**, 134. DOI. ADS.
- Brushlinsky, K.V.: 1989, Computational models in plasma dynamics. In: Dwoyer, D.L., Hussaini, M.Y., Voigt, R.G. (eds.) *Numerical Methods in Fluid Dynamics, Lecture Notes in Physics* **323**, Springer, Berlin, 21. ADS.
- Carlsson, M.: 2007, Modeling the solar chromosphere. In: Heinzel, P., Dorotovič, I., Rutten, R.J. (eds.) *The Physics of Chromospheric Plasmas CS-368*, Astronomical Society of the Pacific, San Francisco, 49. ADS.
- Demoulin, P., Klein, K.-L.: 2000, Structuring of the solar plasma by the magnetic field. In: Rozelot, J.P., Klein, L., Vial, J.-C. (eds.) *Transport and Energy Conversion in the Heliosphere, Lecture Notes in Physics* **553**, Springer, Berlin, 99. ADS.
- Fletcher, L., Turkmani, R., Hudson, H.S., Hawley, S.L., Kowalski, A., Berlicki, A., Heinzel, P.: 2010, Solar flares and the chromosphere. ArXiv e-prints: 1011.4650v2 [astro-ph.SR]. ADS.
- Gabriel, A.H.: 1994, Some problems in understanding the solar corona. In: Rusin, V., Heinzel, P., Vial, J.-C. (eds.) *IAU Colloq. 144: Solar Coronal Structures*, Slovak Academy of Sciences, Tatranska Lomnica, 1. ADS.
- Gary, G.A.: 2001, Plasma beta above a solar active region: Rethinking the paradigm. *Solar Phys.* **203**, 71. DOI. ADS.
- Goodman, M.L.: 2005, Self-consistent magnetohydrodynamic modeling of current sheet structure and heating using realistic descriptions of transport processes. *Astrophys. J.* **632**, 1168. DOI. ADS.
- Haines, M.G.: 2011, A review of the dense Z-pinch. *Plasma Physics and Controlled Fusion* **53**(9), 093001. DOI. ADS.
- Kshevetskii, S.P.: 2006, Study of vortex breakdown in a stratified fluid. *Comput. Math. Math. Phys.* **46**, 1988. DOI. ADS.
- Kshevetskii, S.P., Gavrilov, N.M.: 2005, Vertical propagation, breaking and effects of nonlinear gravity waves in the atmosphere. *J. Atmos. Solar-Terr. Phys.* **67**, 1014. DOI. ADS.
- Leake, J.E., Arber, T.D.: 2006, The emergence of magnetic flux through a partially ionized solar atmosphere. *Astron. Astrophys.* **450**, 805. DOI. ADS.
- LeVeque, R.J.: 1992, *Numerical Methods for Conservation Laws*, 2nd edn. Birkhäuser, Basel.
- Morozov, A.I., Solov'ev, L.S.: 1980, Steady-state plasma flow in a magnetic field. In: Leontovich, M.A. (ed.) *Rev. Plasma Phys.* **8**, Consultants Bureau, New York, 1. ADS.
- Priest, E.R.: 1982, *Solar Magnetohydrodynamics, Geophysics and Astrophysics Monographs* **21**. ADS.
- Schrijver, C.J.: 2001, The coronae of the Sun and solar-type stars (CD-ROM Directory: contribs/schrijv). In: Garcia Lopez, R.J., Rebolo, R., Zapaterio Osorio, M.R. (eds.) *11th Cambridge Workshop on Cool Stars, Stellar Systems and the Sun CS-223*, Astronomical Society of the Pacific, San Francisco, 131. ADS.
- Spitzer, L.: 1962, *Physics of Fully Ionized Gases*, Interscience, New York.
- Thomas, J.P., Roe, P.L.: 1993, Development of non-dissipative numerical schemes for computational aeroacoustics. In: *AIAA 11th Computational Fluid Dynamics Conference, Technical Papers* **2**, Orlando, FL, 906. ADS.

Velikovich, A.L., Clark, R.W., Davis, J., Chong, Y.K., Deeney, C., Coverdale, C.A., Ruiz, C.L., Cooper, G.W., Nelson, A.J., Franklin, J., Rudakov, L.I.: 2007, Z-pinch plasma neutron sources. *Phys. Plasmas* **14**(2), 022701. DOI. ADS.